A multi-wavelength study of the Seyfert 1 galaxy MCG−6-30-15

C. S. Reynolds[1,2], M. J. Ward[3], A. C. Fabian[2] and A. Celotti[4]

[1]JILA, University of Colorado, Boulder, Colorado, CO 80309-0440, USA
[2]Institute of Astronomy, Madingley Road, Cambridge, CB3 0HA
[3]X-ray Astronomy Group, Department of Physics and Astronomy, University of Leicester, Leicester, LE1 7RH
[4]S.I.S.S.A., via Beirut 2-4, 34014 Trieste, Italy

1 February 2008

ABSTRACT

We present a multiwaveband spectroscopic study of the nearby Seyfert 1 galaxy MCG−6-30-15. New optical spectra from the Anglo-Australian Telescope are presented which clearly show the effects of dust extinction/reddening on both the emission line spectrum and the non-stellar AGN continuum. The reddening is constrained to be in the range $E(B-V) = 0.61 - 1.09$. Spectroscopy in the X-ray band, with both *ROSAT* and *ASCA*, reveal absorption by the warm absorber but little or no neutral absorption expected to accompany the dust responsible for the optical reddening. The dusty warm absorber solution to this discrepancy is discussed and photoionization models of such warm absorbers are constructed. The optical spectrum also displays the relatively strong 'coronal' lines of [FeX]λ6375, [FeXI]λ7892 and [FeXIV]λ5303. We show that these lines may plausibly originate from the outer regions of the warm absorber, although better calculations of the collision strengths for these transitions are required in order to conclusively address this issue. We also present new ultraviolet data from the *International Ultraviolet Explorer* and suggest that much of the observed UV flux is scattered into our line of sight (with a scattering fraction of 1–5 per cent). We conclude with a discussion of the global energetics of this system.

Key words: galaxies:active - galaxies:individual:MCG−6-30-15 - X-rays:galaxies

1 INTRODUCTION

Accretion of material onto a supermassive black hole has long been believed to be the fundamental power source of active galactic nuclei (AGN; e.g. see Rees 1984 for a review). However, the physical processes by which the gravitational potential energy of the accretion flow energizes the observed spectrum are still far from certain. Recent spectroscopic studies in the X-ray waveband have shown that, in the innermost regions (i.e. $r \lesssim 10\,\mathrm{R_{Sch}}$; where $\mathrm{R_{Sch}}$ is the Schwarzschild radius of the central black hole) of at least some AGN, there is a geometrically-thin, radiatively-efficient accretion disk (Tanaka et al. 1995; Fabian et al. 1995). A significant fraction of the accretion energy appears to be liberated in a hot, optically-thin, disk-corona which is a prolific radiator of X-rays and γ-rays (probably via the Comptonization of optical/UV photons from the cold accretion disk: Haardt & Maraschi 1991; Field & Rogers 1993; Zdziarski et al. 1994). Although most of the primary radiation is produced in the inner regions of the accretion flow, a significant fraction of this radiation is reprocessed at greater distances from the black hole into UV, optical and IR wavelengths. Studying these reprocessing mechanisms allows the structures surrounding the accreting black hole to be probed and are necessary if we are to disentangle the primary emission from the reprocessed emission.

In recent years, much has been learnt about the various reprocessing mechanisms. It has been realized that approximately half of the X-ray photons emitted from the corona will strike the cold accretion disk, thereby producing 'reflection' features in the X-ray spectrum (Guilbert & Rees 1988; Lightman & White 1988; Pounds et al. 1990). The emission that emerges from these central regions can also be intercepted by more distant structures: these include the broad-line region (BLR), the putative molecular torus of the unified Seyfert schemes and the warm absorber. The scattering of primary radiation into our line-of-sight is also known to be important in at least some AGN. Multi-waveband studies of nearby, bright AGN are invaluable in studying such complex systems.

Many such multi-wavelength studies of AGN have been performed. For example, Alloin et al. (1995) utilized many

ground-based and space observatories to obtain a snapshot (i.e. all data taken almost simultaneously) of the Seyfert 1 galaxy NGC 3783. After careful consideration of possible contaminating sources, these authors fit thermal accretion disk models to the classical big blue bump displayed by this object and hence constrain the black hole mass and accretion rate. They also find an infrared bump which they interpret as thermal emission from hot and warm dust. Many other studies focus on multi-wavelength monitoring in an attempt to map the central engine. For example, extensive monitoring campaigns have been performed on NGC 4151 (Edelson et al. 1996) and NGC 5548 (Korista et al. 1995).

In this paper we perform a multiwaveband study of the nearby Seyfert 1 galaxy MCG−6-30-15 ($z = 0.008$; Pineda et al. 1978; Pineda et al. 1980). Snapshot optical imaging with the *Hubble Space Telescope* (HST) clearly shows this object to be a S0-type galaxy with a bright, nuclear point source. This X-ray bright AGN has recently been the subject of intense spectroscopic study in the X-ray band and so is a good candidate for a multiwavelength study. We present new optical data from the Anglo-Australian Telescope (AAT) and new ultraviolet data from the *International Ultraviolet Explorer* satellite (IUE). Together with archival infrared and X-ray data, this represents the most detailed multiwaveband study of this nearby AGN to date. In particular, we review and reinforce evidence that there is a significant column of dusty ionized material along our line of sight to the central continuum source and BLR, the so-called dusty warm absorber. This material is shown to have a major effect on the observed spectrum of this source.

In Section 2, the data are presented and the basic characteristics at each waveband are discussed. Section 3 examines various estimates for the amount of extinction and absorption towards the central source. A discrepancy between the optical/UV extinction and the X-ray absorption leads us to discuss the possibility of dusty warm absorbers in Section 4. Section 5 probes the connection between the warm absorber and coronal line emission. We discuss our results and their implications for the energetics of the system in Section 6. Section 7 presents our conclusions.

2 THE DATA AND BASIC SPECTRAL PROPERTIES

2.1 Optical

Optical spectra of MCG−6-30-15 were obtained with the AAT on the night of 1995 April 10. The RGO spectrograph with the 300B grating (grating angle 23.27°) was used to obtain blue (3500–5500Å) spectra and the Faint Object Red Spectrograph (FORS) provided red (5700–10000Å) spectra. Red and blue spectra could be taken simultaneously[⋆] via the use of a dichroic beam splitter. The spectral (FWHM) resolutions are ∼ 9Å in the blue and ∼ 30Å in the red. Standard data reduction was performed using the FIGARO software package provided by STARLINK. Wavelength calibration was performed using a Cu-Ar arc. We estimate that

---

[⋆] Due to the shutter configuration and the read-out constraints, the red spectral integrations had to be terminated and read-out 60 s before the blue.

the wavelength calibration is accurate to within 1Å in the blue spectrum and 3Å in the red spectrum. Absolute flux calibration utilized the standard star L745-46A. Finally, the atmospheric water bands within the red spectrum were corrected for using the extremely metal-deficient red giant star HD126587 as a continuum reference source.

In order to be sensitive to intra-night variations in flux or spectrum, we took 18 separate red/blue spectra of MCG−6-30-15. A normal Galactic F-star is situated 6 arcsec to the south of the nucleus of MCG−6-30-15 (Pineda et al. 1980): the slit position was arranged so as to cover both the nucleus and the star. Assuming the star to have a constant flux during the night, this provides a good control against which we can search for flux variations in the nucleus. The exposure time of each spectrum was 600 s in the blue and 540 s in the red.

After reduction it was found that only 8 red/blue spectra were unaffected by the variable weather conditions during the night. The spectrum of the nuclear region of MCG−6-30-15 was extracted from each long-slit spectrum. No significant difference in either overall flux or individual line fluxes could be found between these spectra. Furthermore, no significant variability could be detected when the overall nuclear flux was compared with that of the nearby F-star. These conclusions remain robust even if we include periods of data that were affected by poor weather. We can set upper limits of ∼ 5 per cent on intra-night variation of the optical flux of the nucleus. Given the lack of any detectable variability, the 8 'good' spectra were combined to form a single co-added spectrum with effective exposure times 4800 s in the blue and 4360 s in the red. Figures 1a and 1b show the blue and red coadded spectra, respectively.

These spectra possess extremely high signal-to-noise and, therefore, uncertainties are dominated by calibration effects and atmospheric variations. Comparing the 8 separate good spectra (i.e. those obtained prior to co-adding), we estimate that there is a ∼ 10 per cent uncertainty in the overall normalization of each spectrum. These are most likely due to 'grey' variations in atmospheric conditions. Treating these uncertainties as independent, the coadded spectra should each have an uncertainty of approximately 3 per cent in overall normalization. The uncertainties in the red and blue spectra should be statistically independent.

Several features are immediately apparent from these spectra. The emission line spectrum is dominated by broad Balmer lines (Hα, Hβ, Hγ and Hδ) and narrow forbidden oxygen lines ([OII]λ3727 and [OIII]λ4959/5007). The emission line spectrum, which is clearly related to the Seyfert activity, is examined in more detail below (Section 2.1.2). The spectrum between 9000Å and 10000Å may be severely affected by incorrect subtraction of atmospheric water features, and so the line-like features in this region of the spectrum should be treated with caution. The presence of the Ca II doublet in absorption (near 4000 Å) shows there to be a non-negligible fraction of starlight from the host galaxy contributing to this spectrum. We now examine this stellar component.
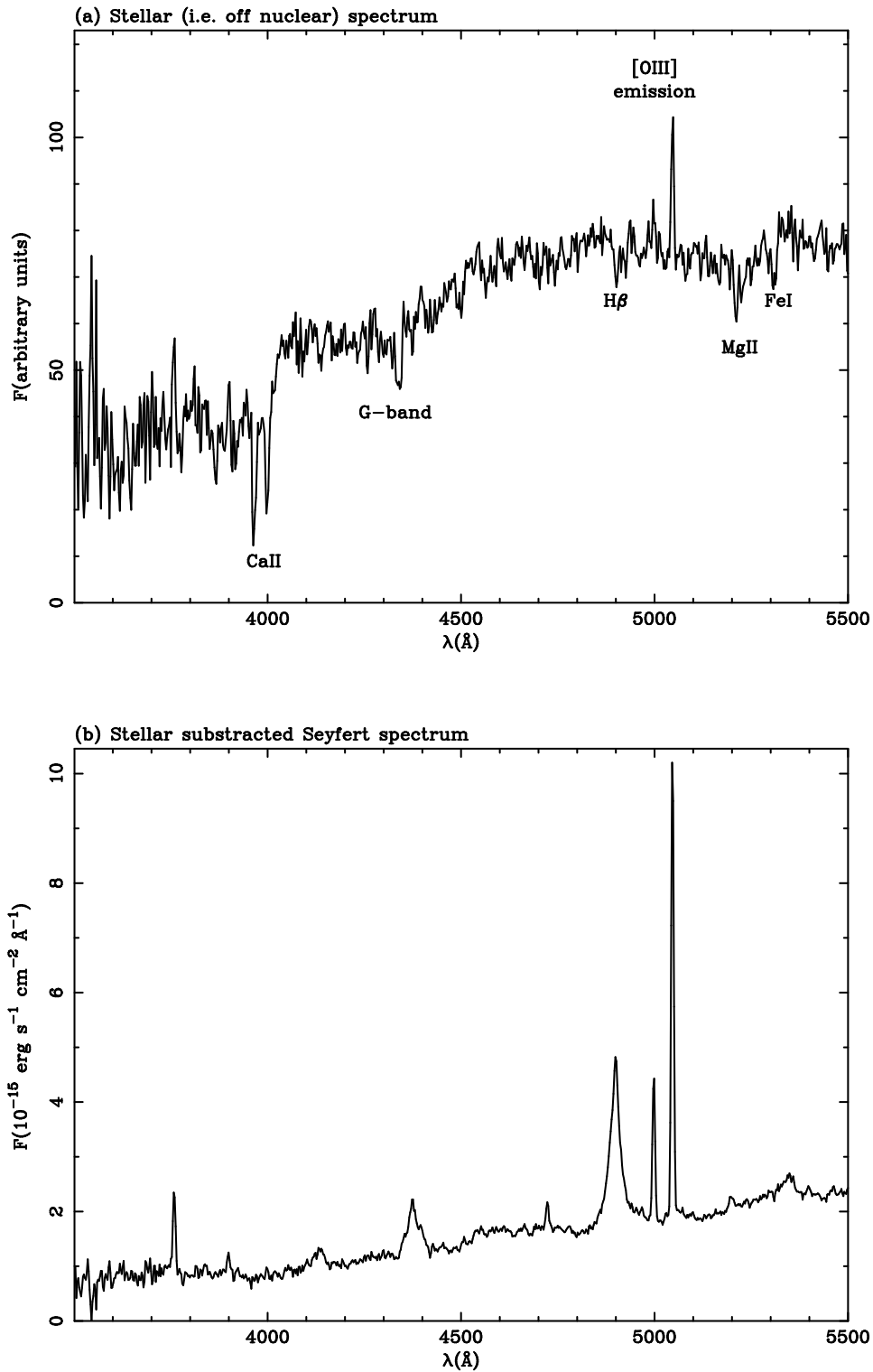
2.1.1 The galactic spectrum

For the blue data we extracted the spectrum of the host galaxy (which appears on the long slit frames as a clearly
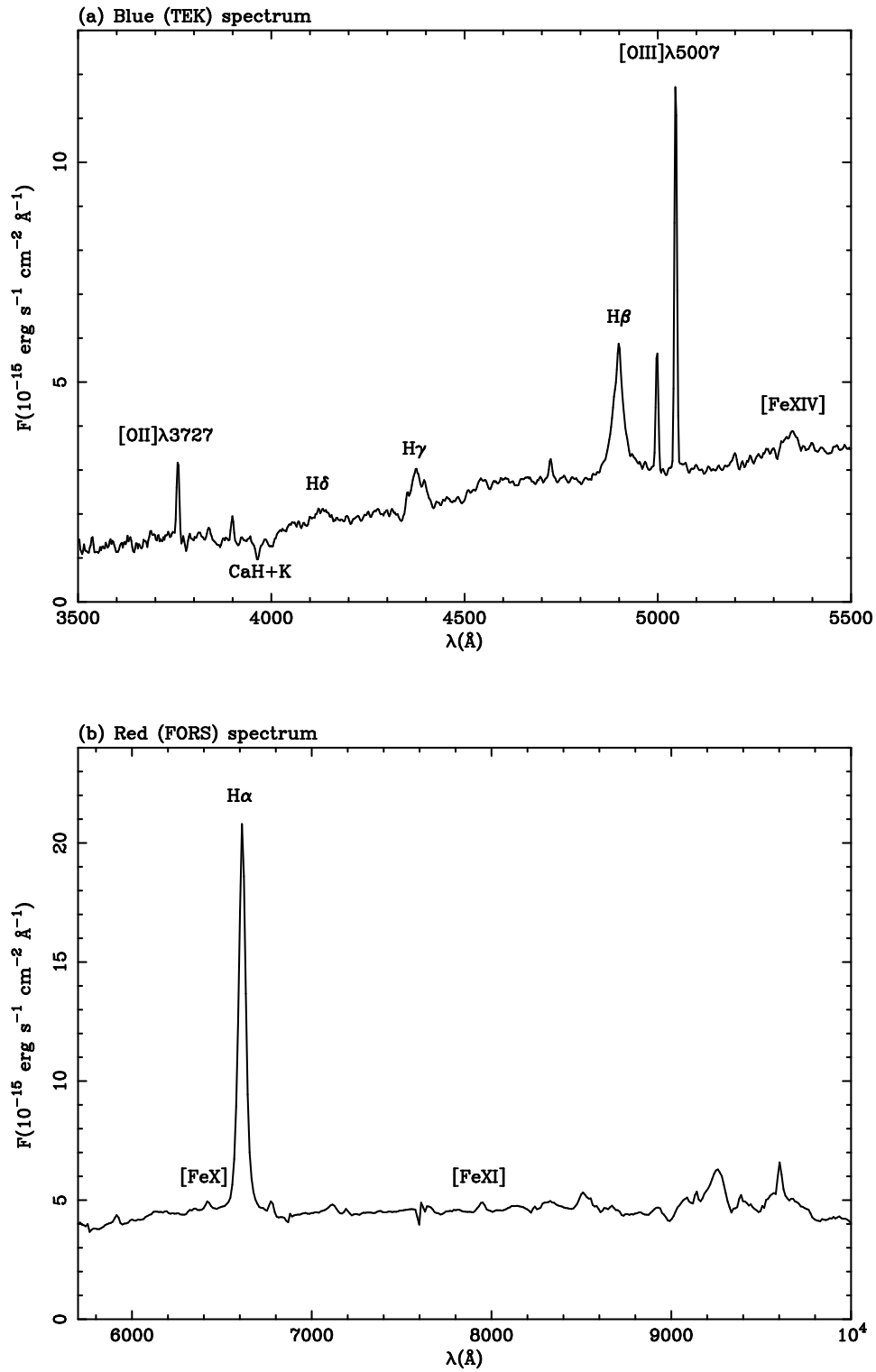
Figure 1. The blue (a) and red (b) optical spectra of the nuclear region of MCG−6-30-15. Prominent emission lines and the Ca II absorption feature have been marked.

Figure 2. a) Spectrum of the off-nuclear, stellar component. The absence of broad Balmer lines, together with the strong redshifted Ca ii doublet feature verifies that the host galaxy has been successfully isolated from the nuclear flux. b) Pure Seyfert spectrum obtained by subtracting the stellar spectrum from the total nuclear spectrum until the Ca ii feature vanishes. Note that the stellar absorption feature of Mg B around 5200Å (rest frame) is also successfully removed.

defined 'fuzz' surrounding the bright nuclear emission.) The spectra extracted from the individual long-slit frames were again co-added to form a single spectrum. Figure 2a shows this co-added spectrum. The absence of any broad Balmer lines from this spectrum is verification that we have successfully isolated the stellar component. Note that there *is* narrow [OII] and [OIII] line emission present in this spectrum. We attribute this to the narrow line region (NLR) possessing significant spatial extent (and therefore contaminating the spectrum of the host galaxy.)

The stellar spectrum reveals several absorption features. The weak Hβ absorption indicates the presence of a young stellar population. An older stellar population give rise to the Mg B, Fe I, G-band and Ca II absorption features.

2.1.2 The nuclear spectrum

Assuming the stellar spectrum to be spatially uniform, we can subtract the spectrum of the host galaxy from the total nuclear spectrum in order to isolate the spectrum of the active nucleus. In practice, we progressively subtract more of the stellar spectrum from the total spectrum until the Ca II doublet feature at ~ 4000Å vanishes. The resulting difference spectrum is taken to be the spectrum of the active nucleus. This is shown in Figure 2b. A similar procedure was not performed for the red (FORS) data because the poorer spatial resolution of our FORS data makes isolation of the host galaxy spectrum more difficult. This would make subtraction of the stellar component rather subjective and consequently diminish its value.

As is typical for Seyfert 1 nuclei, the spectrum consists of a strong non-stellar continuum, broad Balmer lines and narrow permitted and forbidden lines. Both the red and blue spectra were visually examined for known prominent lines. All such identified lines were characterized by fitting a single Gaussian profile whilst modeling the local continuum as a power-law. This procedure was performed on the galaxy-subtracted spectrum, with the exception of those few lines that were identified in the FORS data (for the reasons given above). Since our stellar spectrum is contaminated with forbidden oxygen line emission (presumably from an extended NLR), we note that these oxygen lines will be suppressed by ~ 10 per cent in the galaxy-subtracted AGN spectrum. The single Gaussian parameterization is a (visually) good fit to all of the emission lines except Hβ. Three Gaussian components are required to properly describe this line:

a) A narrow line component at the systemic velocity of the galaxy (defined as the velocity of the [OIII] emission line region) with FWHM$\lesssim 700\,\mathrm{km\,s^{-1}}$ and flux $F_\mathrm{n}(H\beta) = 9.6 \times 10^{-15}\,\mathrm{erg\,cm^{-2}\,s^{-1}}$.

b) A broad line component blueshifted by $200 \pm 60\,\mathrm{km\,s^{-1}}$ relative to the systemic velocity with FWHM$\sim 2400 \pm 200\,\mathrm{km\,s^{-1}}$ and flux $F_\mathrm{b}(H\beta) = 6.3 \times 10^{-14}\,\mathrm{erg\,cm^{-2}\,s^{-1}}$.

c) A very broad line component redshifted by $500 \pm 120\,\mathrm{km\,s^{-1}}$ relative to the systemic velocity with FWHM$\sim 7100 \pm 700\,\mathrm{km\,s^{-1}}$ and flux $F_\mathrm{vb}(H\beta) = 4.6 \times 10^{-14}\,\mathrm{erg\,cm^{-2}\,s^{-1}}$.

The resulting line identifications, wavelengths, line widths and total line fluxes for all of the identified lines are given in Table 1. The errors quoted in this table (and those for the Hβ components above) include both statisti-
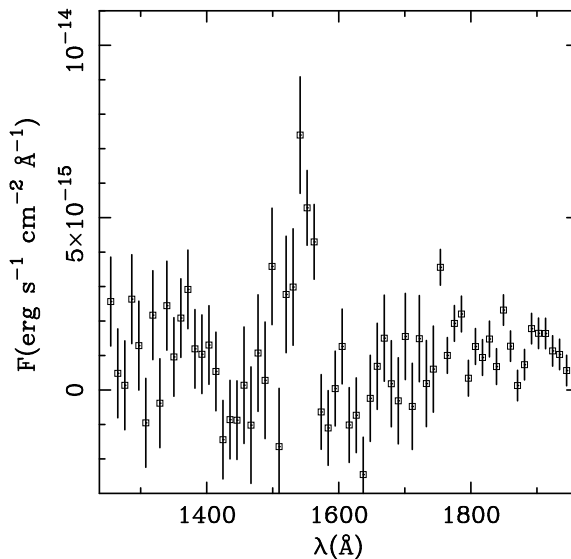
Figure 3. IUE (SWP) data for MCG−6-30-15. Note the weak continuum and the prominent C IVλ1549 line.

cal errors and an estimate of any systematic errors resulting from the wavelength/flux calibration. The statistical errors are derived from χ^2 fitting of the Gaussian models to the data, assuming that the pixel-to-pixel variation is due to random Gaussian noise.

The optical spectrum clearly shows the effect of dust extinction: the continuum flux declines towards the blue end of the spectrum and the Balmer decrements are large. The line-of-sight extinction, and a comparison of this extinction to the line-of-sight X-ray absorption will be addressed in Section 3.

2.2 Ultraviolet

The ultraviolet data were taken by IUE on 1994 July 23–24 (i.e. three days prior to the *ASCA* observation described below.) Due to excessive scattered solar light, we present only the data taken with the short wavelength primary (SWP) camera. These short-wavelength data were taken during one full shift on 1994 July 24 (effective exposure time 8 hours). Data reduction was performed using the ARK software package.

The resulting SWP spectrum is shown in Fig. 3. The source is found to be weak in the UV compared with other wavebands (apart from radio). The hypothesis that this UV spectrum is flat and featureless can be rejected with a high level of confidence: such a hypothesis gives $\chi^2 = 153$ for 65 degrees of freedom (dof). The most significant deviation from the constant model is clearly the C IVλ1549 resonance emission line doublet. Modeling this with a Gaussian profile leads to a highly significant improvements in the goodness of fit ($\Delta\chi^2 = 35$ for 3 additional dof). The inferred properties of this line are reported in Table 1. The C IVλ1549 line appears to be significantly broader than the Hα line, and has a FWHM comparable with the 'very-broad' com-

line identification	rest wavelength (Å)	observed wavelength (Å)	relative velocity of line ($\mathrm{km\,s^{-1}}$)	FWHM ($\mathrm{km\,s^{-1}}$)	line flux ($10^{-15}\,\mathrm{erg\,cm^{-2}\,s^{-1}}$)	equivalent width (Å)
CIV	1549	1545 ± 6	-3000 ± 1200	6200 ± 2100	250 ± 90	140 ± 70
[OII]	3727	3758 ± 1	160 ± 80	< 790	16 ± 2	14 ± 1
[NeIII]	3869	3899 ± 1	-10 ± 80	< 1030	4.3 ± 1.0	4.0 ± 1.5
Hδ	4103	4133 ± 1	-140 ± 70	3000 ± 370	18 ± 4	14 ± 4
Hγ	4342	4374 ± 1	-130 ± 70	2470 ± 180	37 ± 3	30 ± 3
[OIII]	4363	4400 ± 2	210 ± 140	< 1470	5.9 ± 1.2	4 ± 1
HeII	4686	4722 ± 1	-30 ± 60	< 710	5.4 ± 0.6	2.7 ± 0.3
Hβ	4862	see text	see text	see text	119 ± 5	66 ± 3
[OIII]	4959	4997 ± 1	-40 ± 60	< 530	24.0 ± 0.8	11.3 ± 0.3
[OIII]	5007	5046 ± 1	± 60	< 530	83.0 ± 0.7	37.2 ± 0.3
[FeVIII]	5159	5199 ± 1	-10 ± 60	860 ± 160	3.4 ± 0.7	1.4 ± 0.3
[FeXIV]	5303	5343 ± 1	-90 ± 60	2320 ± 300	14 ± 1	5.2 ± 0.4
[FeX]	6375	6422 ± 3	-130 ± 140	1950 ± 500	15 ± 3	$3.0 \pm 0.4^*$
Hα	6563	6613 ± 2	-50 ± 90	2590 ± 90	952 ± 23	$211 \pm 20^*$
[SII]	6712	6775 ± 3	480 ± 130	< 1580	16 ± 3	$3.0 \pm 0.7^*$
[FeXI]	7892	7947 ± 3	-250 ± 110	< 1850	15 ± 3	$3.0 \pm 0.7^*$

Table 1. UV/Optical/NIR line spectrum for MCG−6-30-15. Column 4 shows the velocity redshift of the line centre with respect to the reference frame defined by the [OIII]λ5007 emission ($z = 0.00779$). Column 6 shows the total flux in the line, corrected for Galactic extinction. Those equivalent widths marked with an asterix have been measured from FORS data which have *not* been galaxy-subtracted. All errors and limits are quoted at the 1-σ level.

ponent of the Hβ line. The C IV line is also blueshifted by $\sim 3000\,\mathrm{km\,s^{-1}}$ with respect to the broad Balmer lines. This appears to be a generic feature of high-ionization lines from AGN (e.g. see Espey et al. 1989). This has been interpreted by some authors as evidence for a two-component BLR (e.g. Collin-Souffrin et al. 1988).

There may also be an absorption trough to the blueside of the C IVλ1549 lines. Modeling this with a Gaussian profile leads to a further improvement in the goodness of fit by $\Delta\chi^2 = 12$ for 3 additional dof. According to the F-test, this is not a significant improvement at the 90 per cent level. Thus, we cannot conclusively determine the reality of this feature and shall not discuss it further.

Formally, the best fit continuum level is $F_{\mathrm{SWP}} = (1.1 \pm 0.2) \times 10^{-15}\,\mathrm{erg\,cm^{-2}\,s^{-1}\,\AA^{-1}}$. It is possible that much of this UV continuum could be stellar in origin. Thus, this value should be considered only as an upper limit to the UV continuum flux from the AGN. High-resolution UV imaging with HST will allow the stellar UV flux to be almost completely separated from the AGN UV flux, thereby allowing these two components to be separated. At the time of writing, such UV imaging has yet to be performed.

2.3 Other wavebands

To make this study genuinely multi-waveband in nature, we have supplemented the above new spectra will previously published data. The remainder of this section will introduce these data.

2.3.1 Infrared

Mid/far infrared (MIR/FIR) data were obtained from the *Infrared Astronomy Satellite* (IRAS) Faint Source Catalogue (version 2.0) at four wavelengths ($12\,\mu$m, $25\,\mu$m, $60\,\mu$m and $100\,\mu$m.) Giuricin, Marddirossian & Mezzetti (1995) find good agreement between the IRAS $12\,\mu$m flux and the

ground-based, small-beam $10\,\mu$m (N-band) flux. Thus, it appears there are no strong confusing IR sources in the IRAS beam at the short IRAS wavelengths. Unless there is a very cool confusing source which only reveals itself at the longer IRAS wavelengths, this suggests that IRAS is providing a reliable measurement of the flux of MCG−6-30-15 at all IR wavelengths. Furthermore, this agreement between the ground-based observations and IRAS implies that there is little contribution to the NIR flux from the host galaxy. This is consistent with it being of Hubble type S0.

J-, H-, K- and L-band (i.e. $1.2 - 3.5\mu$m) fluxes were obtained from the ground-based work of Ward et al. (1987).

2.3.2 Soft (0.2–2 keV) X-rays

Soft X-ray data from the *ROSAT* Position Sensitive Proportional Counter (PSPC) were retrieved from the public archive situated at the NASA Goddard Space Flight Center. We chose the longest of the two available PSPC observations of this object. This observation started on 1992-January-29 and collected a total of 8500 s of good data. A PSPC spectrum of MCG−6-30-15 was formed by binning all counts extracted from a circular region of radius 2 arcmin centered on the point source corresponding to MCG−6-30-15. The background count rate within this region is found to be negligible compared with the source.

These data have been previously discussed by Nandra & Pounds (1992). These authors found evidence for a notch in the PSPC spectrum at an energy of $E \sim 0.8\,\mathrm{keV}$. They interpreted this feature as a blend of O VII and O VIII K-shell absorption edges resulting from highly-ionized material along the line of sight to the primary (power-law) X-ray source. This material has become known as the *warm absorber* (Halpern 1984), and shall play a major role in the discussion presented in this paper.

2.3.3 Hard (0.6–10 keV) X-rays

The Advanced Satellite for Cosmology and Astrophysics (*ASCA*) performed a long (4.5-day) observation of MCG−6-30-15 on 1994 July 27. The 'good' exposure times were $\sim 1.5 \times 10^5$ s in each of the four detectors. As a result, high signal-to-noise, medium-resolution X-ray spectra were obtained in the 0.6–10 keV band. The fact that the X-ray flux is highly variable on short timescales, together with *ROSAT* imaging, confirms that the observed X-rays are originating from the central engine of this Seyfert nucleus (see Fig. 1 of Fabian et al. 1995).

Detailed analyses of these data are presented in Tanaka et al. (1995), Otani et al. (1996) and Iwasawa et al. (1996). As discussed by these authors, the 0.6–10 keV X-ray spectrum shows clear deviations from the canonical power-law form. In particular, the O VII and O VIII edges from the warm absorber are prominent features in the 0.7–2 keV range and a broad emission feature is seen between 5–7 keV.

ASCA revealed the warm absorber in MCG−6-30-15 to be highly variable (Fabian et al. 1994; Reynolds et al. 1995; Otani et al. 1996). Detailed modeling of this variability (Otani et al. 1996; Reynolds 1996) has led to a two-zone model for this absorber. There seems to be a highly photoionized inner region (possibly related to the BLR) and a less ionized outer region (possibly related to the putative molecular torus or NLR). It is likely that both of these absorbers are in outflow driven by the radiation pressure of the central source (Reynolds & Fabian 1995).

The emission feature at 5–7 keV is thought to be due to the fluorescent Kα line emission of cold iron (i.e. Fe I–Fe XVII) that results when primary X-rays illuminate cold material in the vicinity of the central engine (George & Fabian 1991; Matt, Perola & Piro 1991). The rest-frame energy of this emission line is 6.4 keV. *ASCA* resolves this line and allows its profile to be determined. It is found that the profile is in good agreement with the hypothesis that it originates from the innermost regions of a thin, radiatively-efficient, accretion disk about a black hole (Tanaka et al. 1995; Fabian et al. 1995; Iwasawa et al. 1996). Relativistic beaming, transverse Doppler shifts and gravitational red-shifts are of major importance in determining the profile of this emission line. From the point of view of the current work, the iron line observation is important since it constrains the geometry of the energetically important inner accretion disk: in the innermost region, much of the energy appears to be liberated as X-rays in an optically-thin region near a radiatively-efficient thin accretion disk viewed at an inclination of 30°.

2.4 The multi-waveband spectrum

The above data are compiled together into a multi-waveband spectrum in Fig. 4. The spectral data plotted in this figure have not been stellar-subtracted or corrected for any reddening (i.e. this is the total galaxy+AGN spectrum as observed at Earth). The dotted line sketches the approximate intrinsic (i.e. dereddened/unabsorbed) spectrum of this source given a reddening of $E(B-V) = 0.61$ (see Section 3).

There are several noteworthy features in this multiwaveband spectrum. First, the observed spectral energy distribution [i.e. $\nu F(\nu)$] peaks in the mid-infrared ($\nu \sim 2 - 3 \times$

10^{13} Hz). As discussed below, this is probably due to thermal emission from warm/hot dust grains. Secondly, whereas many classical Seyfert 1 galaxies display a strong optical/UV continuum (the so-called Big Blue Bump), MCG−6-30-15 is heavily reddened in the optical band and almost extinguished in the UV. There is then a strong recovery at X-ray frequencies. The effect of the warm absorber and iron Kα emission line are clearly seen in the X-ray spectrum.

3 EXTINCTION AND ABSORPTION

The NIR/optical/UV spectrum of MCG−6-30-15 displays the signatures of extinction and reddening by dust. In this section, these signatures are discussed and the amount of reddening is estimated. We then compare the amount of reddening with the observed X-ray absorption.

3.1 Extinction of the optical emission line regions

Extinction by cosmic dust is highly wavelength dependent and hence can change observed line flux ratios significantly away from the intrinsic (i.e. emitted) values. This provides a classic method for determining the amount of dust extinction along the line of sight to a particular emission line region. The relative ratios of the Balmer lines of hydrogen are often used as extinction indicators due to the fact that they are observationally convenient (being in the optical band), strong and their intrinsic relative flux ratios are fairly well determined from atomic theory.

In the case of Balmer lines from AGN, one would ideally deblend the lines into kinematically distinct components, e.g. a broad component (from the BLR) and a narrow component (from the NLR). One could then obtain information about the extinction through to each component. However, high-resolution data is required to facilitate the deblending. To avoid introducing uncertainties due to the deblending procedure we choose to use the total Balmer decrements: thus, the extinction estimates below should be considered as average values over all of the emission line regions.

Table 2 gives the observed Balmer decrements and the expected intrinsic value based upon the assumption of case-B recombination. These decrements have been converted into the reddening, $E(B-V)$, using the standard interstellar extinction curve of Osterbrock (1989). This interstellar extinction curve leads to the expression

$$E(B-V) = a \log \left(\frac{\mathcal{R}}{\mathcal{R}_{\text{intr}}} \right) \tag{1}$$

where $\mathcal{R}$ is the observed Balmer decrement, $\mathcal{R}_{\text{intr}}$ is the intrinsic Balmer decrement and a is a constant which is given in Table 2 for the three Balmer decrements quoted. Table 2 also associates a hydrogen column density, N_{H}, with this reddening. This is given by (Heiles, Kulkani & Stark 1981)

$$N_{\text{H}} = (2.14\pm0.20)\times10^{20} + (3.91\pm0.21)\times10^{21} \, E(B{-}V) \, \text{cm}^{-2} \tag{2}$$

and is the column density of cold gas that would be present under the assumption that the nature of the dust and the cold-gas/dust ratio is the same as is found locally in our Galaxy.
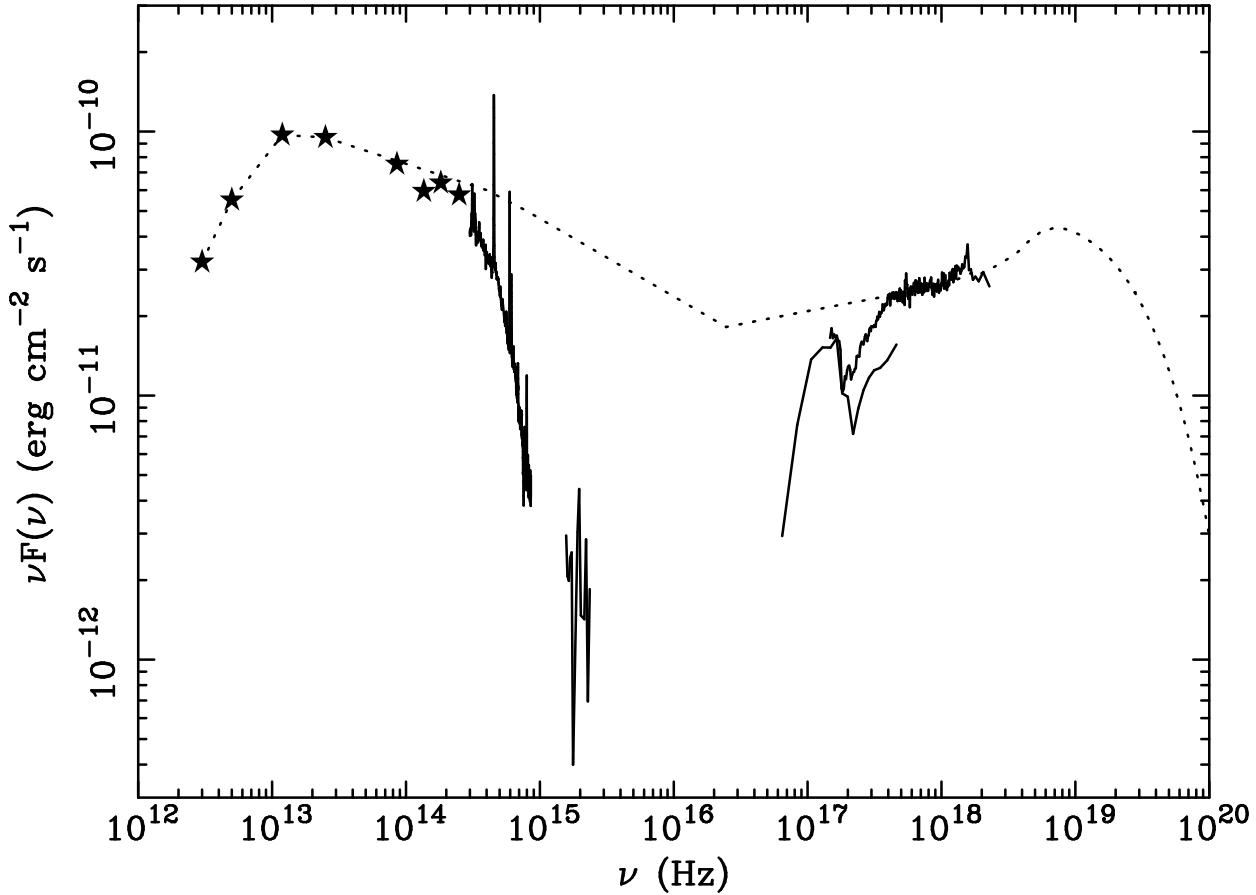
Figure 4. Multiband spectrum of MCG−6-30-15. These data have not been corrected for reddening (either Galactic or intrinsic) and include the stellar component. The dotted line shows the estimated intrinsic spectrum of the source, after correction for reddening and absorption. A reddening of $E(B - V) = 0.61$ (see Section 3) has been assumed in the placement of this line.

Balmer decrement	observed ratio $\mathcal{R}$	intrinsic ratio $\mathcal{R}_{\mathrm{intr}}$	a	$E(B - V)$	N_{H} $(10^{20} \ \mathrm{cm}^{-2})$
Hα/Hβ	8.0 (7.6–8.4)	2.76	2.21	1.02 (0.61–1.09)	42 (26–44)
Hγ/Hβ	0.31 (0.22–0.37)	0.474	−5.17	0.95 (0.56–1.72)	39 (24–69)
Hδ/Hβ	0.16 (0.10–0.26)	0.262	−3.52	0.75 (0–1.47)	31 (0–60)

Table 2. Balmer decrements and inferred extinction for MCG−6-30-15. See text for a discussion of the significance and possible causes of differences between $E(B - V)$ as calculated from difference Balmer decrements. The figures in brackets are the allowed range of the parameter given the various systematic effects discussed in the text.

The calculation of the uncertainties in $E(B - V)$ deserves discussion. We must critically consider both the observational uncertainties and the intrinsic nature of the source.

First, we consider observational uncertainties. The Hα line and Hβ line were measured in different spectrographs, the data from which have undergone independent reduction and calibration. This will introduce some uncertainty into the Hα/Hβ Balmer decrement: in Section 2.1 we estimated that both the red and blue spectra have absolute normalizations which are uncertain to ~ 3 per cent (with these two uncertainties being independent). This leads to a 4–

5 per cent in the Hα/Hβ Balmer decrement, corresponding to an error on the reddening of $E(B - V)_{H\alpha/H\beta} = 1.02 \pm 0.05$. The H$\beta$, H$\gamma$ and Hδ lines all appear in the data from the same spectrograph and so the two independent Balmer decrements that can be formed from these three lines are not sensitive to uncertainties in the overall normalization. However, Hγ and Hδ do suffer from potentially significant observationally-related uncertainties. The Hγ line is blended with the [OIII]λ4363 line and so an unambiguous determination of the Hγ flux, $F(H\gamma)$, is difficult without higher resolution data. By examining ex-

treme cases, we can conservatively bracket $F(H\gamma)$ to the range $(2.8 - 4.3) \times 10^{-14} \, \mathrm{erg \, cm^{-2} \, s^{-1}}$. The corresponding range of inferred reddening is $E(B-V)_{H\gamma/H\beta} = 0.56\text{--}1.72$. The H$\delta$ flux, $F(H\delta)$, is uncertain due to the fact that it is weak compared with the local continuum and so is sensitive to the modeling of that continuum. By examining extreme cases, we can conservatively bracket $F(H\delta)$ to $(1.3 - 3.0) \times 10^{-14} \, \mathrm{erg \, cm^{-2} \, s^{-1}}$. The corresponding range of inferred extinctions is $E(B-V)_{H\delta/H\beta} = 0\text{--}1.47$.

Secondly, we must consider the possibility that the intrinsic Balmer decrements are not well represented by their case-B recombination limits. Deviations from case-B values can occur due to collisional effects and radiative transfer effects which are especially important in the high-density gas found within the BLR. Theoretically, these processes can increase the Hα/Hβ decrement from the case-B value to 10 (Kwan & Krolik 1981) or more (Canfield & Puetter 1981). In these extreme cases, we would not have to postulate any dust reddening towards the emission line regions of MCG−6-30-15 at all. However, observations of other Seyfert 1 nuclei which are thought to be unreddened suggest that intrinsic Hα/Hβ decrements do not exceed 4 (e.g. Malkan 1983; Wu, Boggess & Gull 1983). Using this value of the Hα/Hβ ratio instead of the case-B value decreases the inferred reddening from $E(B-V) = 1.02$ to $E(B-V) = 0.67$. Including the uncertainty in the measured Hα/Hβ ratio, the lower limit to the reddening is $E(B-V) = 0.61$. The effect of deviations from case-B recombination on the intrinsic Hγ/Hβ and Hδ/Hβ have not been investigated in as much theoretical detail as for Hα/Hβ. However, the corresponding uncertainties on the reddening are likely to be insignificant compared with the observational uncertainties discussed above.

To summarize these Balmer decrement studies, the large Hα/Hβ ratio suggests a reddening in the range $E(B-V) = 0.61\text{--}1.09$. This is compatible with the reddening inferred from Hγ/Hβ and Hδ/Hβ although these two Balmer decrements have large uncertainties due to line blending and the modeling of the continuum. Assuming that the cold-dust/gas ratio is similar to that observed locally in our Galaxy, the column density of gas associated with this reddening is in the range $N_{\mathrm{H}} = (2.6 - 4.4) \times 10^{21} \, \mathrm{cm^{-2}}$.

3.2 Extinction of the continuum source

The optical continuum radiation will also be affected by extinction and reddening. Suppose the *intrinsic* spectrum of the (optical) continuum has a form $F_{\mathrm{intr}}(\nu) \propto \nu^{-\alpha}$. Furthermore, suppose that the *observed* (i.e. reddened) optical continuum spectrum is $F_{\mathrm{obs}}(\nu) \propto \nu^{-\alpha_{\mathrm{obs}}}$. The difference between α and α_{obs} is related to the reddening towards the source. From the definition of reddening, it is easily seen that

$$E(B-V) = -2.5 \log\left(\frac{\nu_{\mathrm{B}}^{-\alpha_{\mathrm{obs}}}}{\nu_{\mathrm{V}}^{-\alpha_{\mathrm{obs}}}}\right) + 2.5 \log\left(\frac{\nu_{\mathrm{B}}^{-\alpha}}{\nu_{\mathrm{V}}^{-\alpha}}\right) \quad (3)$$

$$= 2.5(\alpha_{\mathrm{obs}} - \alpha) \log\left(\frac{\nu_{\mathrm{B}}}{\nu_{\mathrm{V}}}\right) \quad (4)$$

$$\approx 0.26(\alpha_{\mathrm{obs}} - \alpha) \quad (5)$$

where ν_{B} and ν_{V} are the frequencies characterizing the B-band and V-band respectively.

Unreddened Seyfert 1 nuclei in the luminosity range

occupied by MCG−6-30-15 tend to have optical continua with $\alpha \sim 2$ (e.g. see study of Morris & Ward 1988, and note that a flat flux spectrum in wavelength space implies $\alpha = 2$ when considered in frequency space). Fitting the (galaxy-subtracted) blue spectrum of the nucleus of MCG−6-30-15, we conclude that α_{obs} lies in the range 4.5–5. Assuming that the intrinsic optical spectrum of MCG−6-30-15 is similar to that found in unreddened Seyfert 1 nuclei, the reddening of the optical continuum source $E(B-V)$ is in the range 0.65–0.78.

The reddening of the optical continuum source is consistent with the lower end of the reddening derived from the Hα/Hβ Balmer ratio. Assuming that the optical continuum is associated with an accretion disk embedded inside the BLR, this result suggests that little dust is present between the accretion disk and the region where the bulk of the the broad line photons are emitted.

3.3 The UV flux – evidence for scattering?

Initially, we shall suppose that the observed C IV line emitting region is seen directly rather than via scattered photons. Furthermore, suppose that the UV continuum and C IV line emission are subject to the same extinction as the optical non-stellar continuum/line regions. Since we have determined the optical reddening to be in the range $E(B-V) = 0.61 - 1.09$, we can deredden the C IV line in order to estimate its intrinsic (i.e. dereddened) flux. Thus, *given this supposition that the UV line emitting region is seen directly*, we constrain the intrinsic C IV line flux to lie in the range

$$F_{\mathrm{intr}}(CIV) = (1.4 - 102) \times 10^{-11} \, \mathrm{erg \, cm^{-2} \, s^{-1}}, \quad (6)$$

where we have included the 1-σ errors in the observed flux and used the UV extinction law of Osterbrock (1989). This is a rather large line flux, corresponding to an isotropic luminosity of $3 \times 10^{42} \, \mathrm{erg \, s^{-1}}$ or greater in the C IV line alone.

To quantitatively assess how large this line flux is, consider the lower end of this range corresponding to $E(B-V) = 0.61$. For this reddening, the dereddened Hβ flux is

$$F_{\mathrm{intr}}(H\beta) = 9.1 \times 10^{-13} \, \mathrm{erg \, cm^{-2} \, s^{-1}}, \quad (7)$$

leading to a lower limit on the intrinsic C IV/Hβ flux ratio of 15. This ratio is very sensitive to the reddening assumed and can *greatly* exceed this value if $E(B-V) > 0.61$. In unreddened Seyfert nuclei, this ratio is often significantly smaller. For example, in the AGN Watch Campaign on NGC 3783, the intrinsic C IV/Hβ flux ratio is ~ 10 (Reichert et al. 1994; Stirpe et al. 1994). Similarly, the C IV/Hβ flux ratios found during the monitoring campaigns on NGC 4151 (Crenshaw et al. 1996; Kaspi et al. 1996) and NGC 5548 (Korista et al. 1995) are ~ 7 and ~ 9, respectively.

We must conclude that the C IV line flux is unusually high compared with the optical line fluxes, or that one of our assumptions has broken down. There are three possible ways that our above argument might be flawed. First, source variability during the 9 months separating the UV and optical observations may produce an apparently unusual line ratio, even if the intrinsic line ratio is normal. In our minimum reddening case ($E(B-V) = 0.61$), only mild variability (~ 30 per cent over 9 months) is required to make the observed C VI/Hβ ratio of 15 consistent with the that

seen in other objects. As one postulates higher reddening values, the more extreme is the inferred intrinsic line ratio and the more violent the variability needed. Secondly, the reddening towards the high-ionization BLR (including the C IV line emitting region) may be different than that towards the low-ionization BLR (which includes the Balmer line emitting region). Whilst this is clearly a viable possibility (and one can imagine central-engine geometries that produce such an effect) there is no precedent for the high-ionization BLR to be less reddened than the low-ionization BLR. Thirdly, some fraction of the photons from the BLR might be scattered around the material responsible for the extinction. If the scattering fraction is wavelength independent (e.g. electron scattering), the scattering will tend to preferentially enhance the UV relative to the optical due to the fact that the *direct* flux is heavily reddened. Since we know scattering to be an important process in some other Seyfert nuclei, we now explore this last possibility in more detail.

Suppose that the intrinsic UV/optical line spectrum is similar to that of NGC 3783, with a C IV/Hβ flux ratio of 10. We can write the observed fluxes of both of these lines, $F_{\rm obs}$, as a sum of the direct (extinguished) flux and the scattered flux which is assumed not to suffer any extinction beyond that due to Galactic material. If f is the scattering fraction, then we have

$$F_{\rm obs} = \left(10^{-bE_{\rm Gal}(B-V)}f + 10^{-bE(B-V)}\right) F_{\rm intr} \qquad (8)$$

where b is a parameter dependent on the extinction law used. The standard interstellar extinction curve of Osterbrock (1989) gives $b = 3.2$ for C IVλ1549 and $b = 1.45$ for Hβ. The first term on the right hand side of equation (8) represents the scattered flux including the effects of extinction by Galactic material. We take $E_{\rm Gal}(B - V) = 0.06$ (Berriman 1989). The second term of equation (8) gives the contribution due to the direct (extinguished) flux. Dividing these equations for C IVλ1549 and Hβ gives a relation between the required scattering fraction f and the total line-of-sight reddening $E(B - V)$. This relationship is shown in Fig. 5 for interesting values of $E(B - V)$. It can be seen that scattering fraction of between 1–5 per cent (depending on the total reddening) are required in order to make the observed line ratios consistent with an intrinsic C IV/Hβ line ratio of 10.

3.4   X-ray absorption

X-rays are thought to be produced in the very central regions of the accretion disk. The absorption of those X-rays by line-of-sight material is readily observable at soft X-ray energies and provides important information on the surroundings of the active nucleus. The discussion of X-ray absorption is commonly divided into that of 'cold' absorption (i.e. by neutral material) and 'warm' absorption (i.e. by ionized material).

The warm absorption has already been discussed in Sections 2.3.2 and 2.3.3. As previously mentioned, variability studies have led to a two-zone model for this absorber. Table 3 summarizes the properties of these two absorbing regions based on modeling with the photoionization code CLOUDY (Ferland 1991).
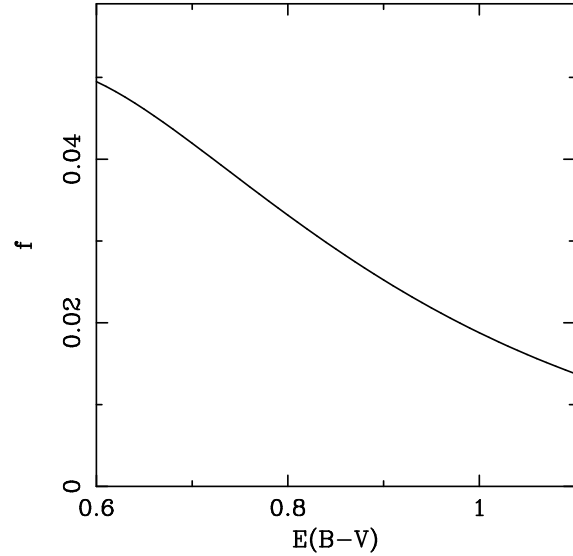
Figure 5. Relationship between the required scattering fraction, f, and the total line-of-sight reddening, $E(B - V)$, assuming an intrinsic C IVλ1549/Hβ flux ratio of 10.

property	inner absorber	outer absorber
$N_{\rm W}$ (10^{20} cm^{-2})	130	46
ξ (erg cm s^{-1})	74	17
density $n_{\rm e}$ (10^5 cm^{-3})	$\gtrsim 20$	$\lesssim 2$
distance R (pc)	≈ 0.005	$\gtrsim 1$
temperature T (10^5 K)	5	0.5
[FeX]$_{\rm model}$/[FeX]$_{\rm obs}$	$4 \times 10^{-5} f_{\rm c}$	$24 f_{\rm c}$
[FeXI]$_{\rm model}$/[FeXI]$_{\rm obs}$	$4 \times 10^{-6} f_{\rm c}$	$0.5 f_{\rm c}$
[FeXIV]$_{\rm model}$/[FeXIV]$_{\rm obs}$	$0.04 f_{\rm c}$	$24 f_{\rm c}$

Table 3. Properties of the warm absorbers in MCG$-$6-30-15.

Once the effect of the warm absorber has been modeled, the X-ray spectrum can be examined for evidence of additional cold absorption in excess to that expected from our own Galaxy (the Galactic column density along the line of sight to this source is $N_{\rm Gal} = 4.1 \times 10^{20}$ cm^{-2}). Describing the warm absorber with a simple one-zone photoionization model computed by the code CLOUDY (see Fabian et al. 1994 for a detailed description of this warm absorber model), the *ASCA* spectrum suggests an excess cold column density of $N_{\rm H} = 1.7^{+0.4}_{-0.3} \times 10^{20}$ cm^{-2}. Quoted errors are statistical in nature and stated at the 90 per cent confidence level for one interesting parameter ($\Delta\chi^2 = 2.7$). It has been suggested that the low energy calibration of the *ASCA* SIS is incorrect so as to over-estimate the cold absorption by 1–3×10^{20} cm^{-2} (e.g. see discussion in Cappi et al. 1997). Thus, within these calibration uncertainties, our result may be consistent with there being negligible cold absorption excess to the Galactic column. Fitting the same simple model to the *ROSAT* PSPC spectrum suggests an excess column density of $N_{\rm H} = (1.9 \pm 0.3) \times 10^{20}$ cm^{-2}, in good agreement with the *ASCA* result.

3.5   The absorption/reddening mis-match

Comparing the results of Sections 3.1–3.4 reveals an apparent contradiction. X-ray observations show that the column density of cold (neutral) gas along the line of sight to the primary X-ray source is $N_{\rm H} \lesssim 2 \times 10^{20} \, {\rm cm}^{-2}$. However, both the optical continuum source and the BLR are highly reddened. On the basis of local (Galactic) studies, we would expect a cold gas column density of $N_{\rm H} \gtrsim 2.6 \times 10^{21} \, {\rm cm}^{-2}$ to be associated with the dust responsible for the reddening. This is more than an order of magnitude above the X-ray limits. Since the X-ray emission is thought to occur deeper within the central engine than either the optical continuum or optical line emission, this result is somewhat surprising.

This discrepancy for MCG−6-30-15 was first hinted at by Pineda et al. (1980) and explicitly commented upon by Reynolds & Fabian (1995) on the basis of data drawn from the literature. A similar discrepancy has been found for IRAS 13349+2438 (Brandt, Fabian & Pounds 1996), an infrared luminous quasar which also displays a prominent warm absorber. These authors discuss various resolutions of this discrepancy. To summarize these discussions, it is found that the only way to reconcile this result with a plausible geometry and a physically reasonable gas-to-dust ratio is to suggest that the dust resides in the *ionized* gas that constitutes the warm absorber. The soft X-ray opacity of this material is less than that of cold material primarily due to the almost complete ionization of hydrogen and helium. The dusty warm absorber hypothesis has also been explored by Reynolds (1997) in the context of a sample of Seyfert galaxies. We now discuss dusty warm absorbers in more detail.

4   DUSTY WARM ABSORBERS

In this section we explore the idea of a dusty warm absorber in more detail than any of the above previous work. In particular, we construct photoionization models of dusty warm absorbers and explicitly fit these models to the *ASCA* data.

4.1   Dust survivability

Dust grains are highly efficient radiators and hence can thermally decouple from the surrounding hot gas. Under the conditions envisaged here, there are two grain destruction mechanisms that must be considered. First, if the grains themselves become too hot, they will rapidly sublime. The grain temperature will be set by the thermal equilibrium between the AGN radiation incident on a given grain and the thermal radiation emitted by that grain (e.g. see Barvainis 1987). For MCG−6-30-15, the *sublimation radius* (i.e. the radius from the AGN within which dust grains become so hot that they sublime) is $\sim 10^{17} \, {\rm cm}$. Thus, any dust grains within the inner warm absorber would be rapidly sublimed by the intense radiation field. Dust in the outer warm absorber would not be subject to significant sublimation.

The second dust destruction mechanism that we must consider is thermal sputtering. If we make the standard assumption that the (outer) warm absorber is photoionized, then photoionization models suggest that the gas temperature is only $T \sim 5 \times 10^4$ K and thermal sputtering is negligible. If, instead, we suppose that the outer warm absorber is

purely collisionally-ionized, gas temperatures of $T \sim 10^6$ K are required in order to achieve the observed ionization states (Shull & van Steenberg 1982). From the expressions of Burke & Silk (1974), the thermal sputtering timescale for this temperature is

$$t_{\rm sp} \approx 3 \times 10^6 \left(\frac{n}{1 \, {\rm cm}^{-3}} \right)^{-1} \, {\rm yr}, \qquad (9)$$

where n is the electron number density in the gas. Suppose that r is the distance of the outer warm absorber from the central engine, and L is the (ionizing) luminosity of the central engine. Furthermore, define $\xi_{\rm equiv} \approx 20 \, {\rm erg \, cm \, s}^{-1}$ to be the ionization parameter of a photoionized plasma in which oxygen is ionized to the same degree as seen in the outer warm absorber of MCG−6-30-15. Given our (temporary) hypothesis that the plasma is collisionally-ionized, the density must satisfy

$$n > \frac{L}{\xi_{\rm equiv} r^2}, \qquad (10)$$

or else photoionization would dominate the ionization state. Evaluating the sputtering timescale for the parameters of MCG−6-30-15 gives

$$t_{\rm sp} \lesssim 10 \left(\frac{r}{1 \, {\rm pc}} \right)^2 \, {\rm yr}. \qquad (11)$$

For comparison, the flow timescale of the outer warm absorber is

$$t_{\rm flow} \sim \frac{r}{v_{\rm flow}} \sim 10^3 \left(\frac{r}{1 \, {\rm pc}} \right) \, {\rm yr}, \qquad (12)$$

where we have adopted a typical value of $v_{\rm flow} = 1000 \, {\rm km \, s}^{-1}$ for the velocity of the outer warm absorber, as indicated by UV absorption line studies of other AGN (Mathur, Elvis & Wilkes 1995). It can be seen that the flow timescale of the warm absorber always exceeds the sputtering timescale unless $r \gtrsim 100$ pc. If the outer warm absorber was situated at such a large distance, then either we would have to be viewing the AGN along a very special line of sight, or else the mass, M, and kinetic energy, $L_{\rm K}$, associated with the outflow would both be huge. From the expressions of Reynolds & Fabian (1995), and assuming a global covering fraction of $f_{\rm c} = 0.1$, we get $M \sim 10^6 \, {\rm M}_\odot$ and $L_{\rm K} \sim 3 \times 10^{42} \, {\rm erg \, s}^{-1}$. The initial acceleration of this material would be extremely problematic to understand. We consider this possibility to be unphysical. Thus, in the absence of a viable, collisionally-ionized model, *the observation of a dusty warm absorber may be taken as further evidence that photoionization dominates the state of this plasma.*

Whilst dust can survive in warm photoionized gas, it is extremely difficult to form dust in such an environment: the grains could never assemble at such temperatures. Furthermore, a comparison of the column density of the warm absorber with the cold column expected to be associated with the reddening reveals that the warm-gas/dust ratio in the warm absorber must be very similar to the cold-gas/dust ratio in our Galaxy. These two facts taken together suggest that the warm material originates from dusty cold material, possibility via radiative heating, and that a substantial fraction of the dust survives the heating process. The putative dusty molecular torus of Seyfert unification schemes might

model parameter	standard dust mixture	graphite dust only
$N_{\mathrm{W,outer}}(10^{20}\,\mathrm{cm}^{-2})$	$47.1^{+2.9}_{-2.0}$	$57.5^{+5.6}_{-3.8}$
$\xi(\,\mathrm{erg\,cm\,s}^{-1}\,)$	$25.1^{+3.8}_{-0.3}$	$19.5^{+2.6}_{-2.3}$
Γ	$2.17^{+0.02}_{-0.04}$	$2.13^{+0.02}_{-0.02}$
χ^2/dof	$430/229$	$362/229$

Table 4. Results of fitting dusty warm absorber models to *ASCA* data.

be a possible progenitor of such a radiatively-driven, warm, dusty outflow.

4.2 Photoionization models

We have constructed photoionization models of dusty warm absorbers using the photoionization code CLOUDY. Grids of such models were constructed for various values of the column density N_{W}, ionization parameter ξ and X-ray photon indices Γ. Since we are interested in the behaviour of the outer warm absorber, the distance of the absorber from the primary source was fixed at 1 pc. Otherwise, these models are identical to those of Fabian et al. (1994) and Reynolds et al. (1995) except for the inclusion of dust grains. The grain models used are described in HAZY (the manual to CLOUDY) pp. 284. Prompted by the observations of the previous paragraph, we have fixed the gas/dust ratio to Galactic value. Two such grids were computed: one contains a standard (i.e. local) mixture of silicate and graphite grains whereas the other contains only graphite grains.

These models were fitted to the *ASCA* data. Since we are interested in modeling fine details of the soft *ASCA* spectrum, only data from the best calibrated solid-state imaging spectrometer (SIS0) were used in the spectral fitting process. Furthermore, only data in the range 0.6–4 keV were fitted: below 0.6 keV the *ASCA* calibration becomes uncertain whereas above 4 keV spectral complexities due to the Fe Kα line become relevant. In detail, our spectral model has three components. First, the primary power-law and the *outer* warm absorber are modeled using CLOUDY as described above. Secondly, the effect of the *inner* warm absorber was modeled as a O VIII absorption edge with (rest-frame) threshold energy 0.87 keV and optical depth at threshold of $\tau_{\mathrm{O8}} = 0.18$ (Otani et al. 1996)[†]. Lastly, Galactic absorption by a cold column of $N_{\mathrm{H}} = 4.06 \times 10^{20}\,\mathrm{cm}^{-2}$ was included. The spectral fitting results are shown in Table 4.

Table 4 shows that the assumed dust composition has a significant effect on the goodness of fit. The model which assumes graphite grains only is a much better fit than the model with a standard dust mixture ($\Delta\chi^2 = 68$ for the

same number of dof). The reason for this difference is illustrated in Fig. 6 which shows the best-fit unfolded model and the 0.6–2 keV SIS0 data for each of the two assumed dust compositions. The standard dust model predicts a large photoelectric K-edge due to neutral oxygen (threshold energy 0.533 keV). Such an edge is not observed. The graphite grain model predicts a significantly smaller neutral oxygen edge which is much more consistent with observations. Note that the neutral oxygen edge in the latter model originates purely from the Galactic column and not from the dusty warm absorber. Thus, the graphite grain model seems to be preferred over the standard dust mixture model.

The signatures of dust in a dusty warm absorber only become significant at X-ray energies below the *ASCA* band. Thus, we must check that the dusty warm absorber model is consistent with the soft X-ray spectrum as determined by the *ROSAT* PSPC. In detail, we compared the *ROSAT* PSPC data with a spectral model consisting of a power-law form (photon index Γ) absorbed by three components:

a) a dusty warm absorber model as computed by CLOUDY (column density N_{W} and ionization parameter ξ),

b) an absorption edge at the threshold energy of O VIII to mimic the effect of the dust-free inner warm absorber (optical depth at threshold τ_{O8}),

c) neutral absorption to account for Galactic and intrinsic cold gas absorption (column density N_{H}).
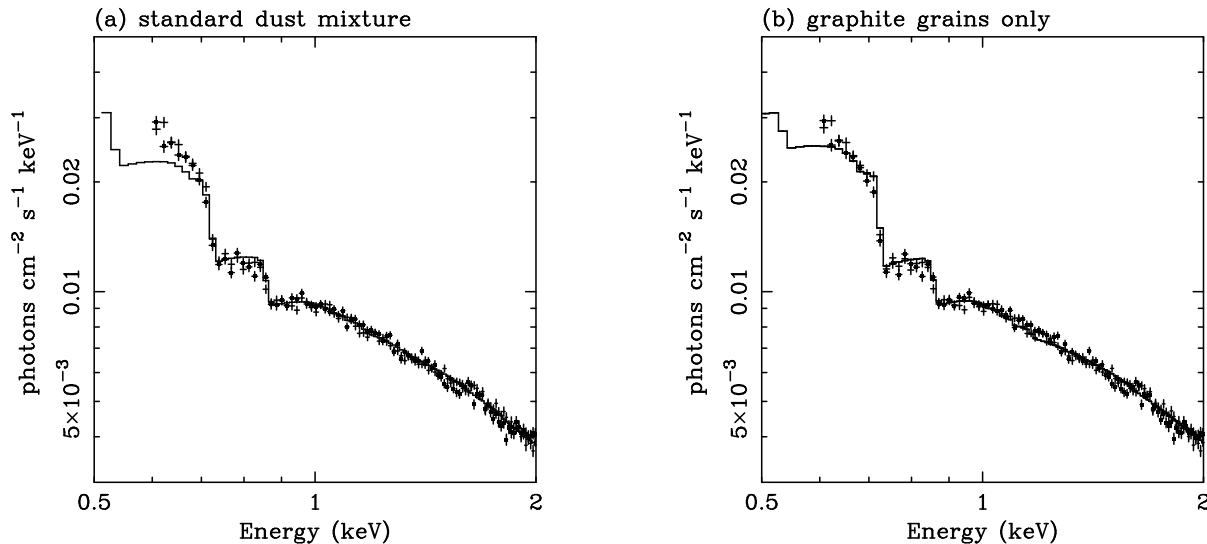
This 6 parameter scheme over-models the *ROSAT* PSPC spectrum (which has ~ 5 independent energy channels). Thus, we do not formally fit the data since any such fit is very poorly constrained – we merely seek to demonstrate consistency with the fit parameters derived from the *ASCA* data. Both the standard dust and the graphite dust warm absorber models are found to be consistent with the PSPC data for the following parameters: $\Gamma = 2.8$, $N_{\mathrm{W}} = 4.5 \times 10^{21}\,\mathrm{cm}^{-2}$, $\xi = 20\,\mathrm{erg\,cm\,s}^{-1}$, $\tau_{\mathrm{O8}} = 0.83$, $N_{\mathrm{H}} = 6.9 \times 10^{20}\,\mathrm{cm}^{-2}$. These parameters are roughly consistent with those derived from the *ASCA* data with the exception of Γ and τ_{O8}. We will briefly address these in turn.

First, the photon index Γ is inferred to be significantly steeper in the *ROSAT* observation than the *ASCA* observation. At least some of this discrepancy ($\Delta\Gamma \sim 0.5$) may be due to previously noted errors in the *ROSAT*–*ASCA* cross-calibration. However, there may be a true softening of the X-ray spectrum in the *ROSAT* band due to the onset of a soft excess. It must be noted that the *ASCA* data do not show any evidence of a soft excess above 0.6 keV (Reynolds 1997). Temporal variations of Γ may also explain such a discrepancy (note that the *ROSAT* and *ASCA* observations are separated by over 2 years).

Secondly, the O VIII edge depth τ_{O8} is inferred to be significantly deeper in the *ROSAT* observation than in *ASCA* observation. This can be understood as a real (i.e., physical) change. Otani et al. (1996) and Reynolds (1996) have found a relationship between the instantaneous value of τ_{O8} (as measured by *ASCA*) and the luminosity of this source. From the analysis of Reynolds (1996), this relation takes the form

$$\tau_{\mathrm{O8}} \approx 0.12 \left(\frac{L_{2-10}}{10^{43}\,\mathrm{erg\,s}^{-1}} \right)^{-2.7} \qquad (13)$$

where L_{2-10} is the 2–10 keV luminosity of the source. This can be understood physically in terms of a highly-ionized

---

[†] Short term spectral variability in the soft *ASCA* band is known to occur during this observation (Otani et al. 1996), and one might worry about the effect of this variability when one performs spectral fitting on the time-averaged spectrum. However, it is known that changes in τ_{O8} dominate this spectral variability. Thus, the best fitting parameters for the outer warm absorber (which contributes very little to the O VIII edge) should be relatively unaffected by spectral variability

(a) standard dust mixture   (b) graphite grains only

Figure 6. Dusty warm absorber models fitted to 0.6–4 keV data from the *ASCA* SIS0 (plain crosses). SIS1 data are also shown (filled squares) but have not been used in the spectral fitting reported in Table 4. Panel a) shows the model computed with a standard (i.e. Galactic) mixture of graphite and silicate dust grains. Panel b) shows the model computed with only graphite grains.

warm absorber in which most of the oxygen atoms are fully stripped of all electrons (i.e. O IX is the dominant state). A drop in ionizing luminosity results in an increased number of O VIII ions due to recombination of the O IX ions. This produces the observed anti-correlation between τ_{O8} and L_{2-10}.

During the *ROSAT* observation, the average 2–10 keV luminosity is in the range $L_{2-10} = 4 - 8 \times 10^{42} \, \mathrm{erg \, s^{-1}}$. The large uncertainty in luminosity is due to the uncertainty in the extrapolation from the *ROSAT* band to the 2–10 keV band. The corresponding range of edge depth is $\tau_{O8} = 0.2 - 1.4$. Thus, the value needed to agree with the *ROSAT* spectrum, $\tau_{O8} = 0.83$, is completely consistent with this relationship.

To summarize these X-ray results, we have shown that a warm absorber containing sufficient dust to explain the optical reddening is also compatible with the *ASCA* and *ROSAT* data. In principle, a detailed examination of the neutral K-edges of the various dust-phase metals allows the composition of the dust to be probed. Although it is extremely hard to make definitive statements yet due to the lack of high-quality soft X-ray spectra, there is evidence that the dust grain composition is non-standard in so far as it contains few silicate grains. We note that due to the tentative nature of this conclusion, we have not taken account of any non-standard dust composition when performing the reddening calculations of Section 3. Clearly, this should be the subject of future work.

4.3   Dust emission and the infrared bump

The multiwaveband spectrum of MCG$-$6-30-15 clearly shows a large IR bump. If this infrared bump is interpreted as the thermal emission from dust grains, the corresponding grain temperature is $T \sim 300 - 500 \, \mathrm{K}$. The fact that the $25 - 100\mu\mathrm{m}$ fluxes describe an approximate Rayleigh-Jeans form shows that dust cooler than $T \sim 300 \, \mathrm{K}$ cannot

contribute much to the observed emission. However, the relatively flat $12 - 25\mu\mathrm{m}$ spectrum shows that there are probably hotter dust components. Here we investigate whether this IR bump can be understood as thermal emission from a dusty warm absorber.

Following the work of Barvainis (1987), we calculate the mass of dust required to produce the $12\mu\mathrm{m}$ flux observed in MCG$-$6-30-15. Assuming graphite grains with a radius of $a = 0.05\mu\mathrm{m}$, a density of $\rho = 2.26 \, \mathrm{g \, cm^{-3}}$ and temperature of $T = 500 \, \mathrm{K}$, we estimate that $15 \, \mathrm{M_\odot}$ of dust is required to produce the $12\mu\mathrm{m}$ flux. Furthermore, assuming a standard gas-to-dust mass ratio of 200, the corresponding mass of associated gas is $3000 \, \mathrm{M_\odot}$. If, instead, we consider a grain temperature of $T = 1500 \, \mathrm{K}$, the increased dust emissivity lowers the dust mass requirement to $6 \, \mathrm{M_\odot}$ with a corresponding gas mass of $1200 \, \mathrm{M_\odot}$.

The mass of the outer (dusty) warm absorber can be independently estimated from simple arguments using the X-ray data. Approximating as a thin, uniform, spherical shell, the mass of ionized plasma is

$$
\begin{aligned}
M & = 4\pi R^2 N m_\mathrm{p} f_\mathrm{c} & (14) \\
& \approx 1000 \, R_\mathrm{pc}^2 N_{22} f_\mathrm{c} \, \mathrm{M_\odot} & (15)
\end{aligned}
$$

where $R = R_\mathrm{pc} \, \mathrm{pc}$ is the radial distance of the absorbing region, $N = 10^{22} N_{22} \, \mathrm{cm^{-2}}$ is the column density and f_c is the covering fraction of the material as seen from the central source (i.e. the 'global' covering fraction). In MCG$-$6-30-15, we must have $R_\mathrm{pc} \lesssim 1$ in order to heat the dust to $T \gtrsim 500 \, \mathrm{K}$. The *ASCA* data directly constrain the column density to be $N_{22} \sim 0.5$. Thus, we have

$$
M \lesssim 500 \, f_\mathrm{c} \, \mathrm{M_\odot} \tag{16}
$$

with only f_c remaining unconstrained. This is somewhat less than the mass derived in the previous paragraph, especially when it is noted that there are arguments suggesting $f_\mathrm{c} \sim 0.1$ (see Reynolds 1997 and Section 5.)

The disagreement between these two mass estimates is not unexpected. We would only expect agreement if most of the warm/hot dust emission originated from grains in a warm absorber which approximated a uniform spherical shell. Realistically, a rather more complicated geometry would be expected. In particular, large quantities of warm/hot grain emission would be expected from dusty gas associated with the irradiated inner edge of the putative dusty molecular torus. Indeed, it may be artificial to consider the outer warm absorber and the torus as distinct and separate entities – the outer warm absorber may well be an optically-thin, outflowing extension of the standard (optically-thick) cold torus.

5   HIGH-IONIZATION (CORONAL) EMISSION LINES

The optical spectrum of MCG−6-30-15 clearly displays the very high-excitation forbidden lines of [FeX]λ6375, [FeXI]λ7892 and [FeXIV]λ5303. These are the so-called iron coronal lines. Previous studies of the coronal lines in Seyfert galaxies have found them to have line widths intermediate between that of the lower-excitation forbidden narrow lines (such as [OIII]) and the permitted broad lines (Grandi 1978). These studies have also found the coronal lines to be slightly blueshifted with respect to the narrow forbidden lines. As shown in Table 2, the coronal lines in MCG−6-30-15 follow exactly these trends. Note that the true width and flux of the [FeXIV]λ5303 line may be less than that presented in Table 2 due to blending with [CaV]λ5309. Oliva et al. (1994) have examined various models for the coronal line emission.

Such observations have led to the discussion of the coronal line region (CLR) which is distinct from the BLR or NLR. Here we address the possibility that the CLR in MCG−6-30-15 can be identified with the outer warm absorber.

The collision strengths for these transitions are poorly known (Osterbrock & Fulbright 1996; Oliva 1996). Any calculations of line strengths that we perform will be tainted by this basic uncertainty in the atomic physics. Despite these uncertainties, we have used CLOUDY to examine the coronal line emission from the inner and outer warm absorber. Table 3 reports the predicted coronal line fluxes as a fraction of the observed line flux. These predicted fluxes assume an optically-thin, unobscured spherical shell with total covering fraction f_c.

It is clear from Table 3 that the inner warm absorber cannot contribute much to the observed coronal line emission. This is primarily due to the fact that iron is too highly ionized, although collisional de-excitation is also relevant in suppressing the coronal line emission. On the other hand, the outer warm absorber can produce significant coronal emission. If we hypothesize that all of the [FeX]λ6375 and [FeXIV]λ5303 emission originates from the outer warm absorber, we deduce that $f_c \approx 0.04$. However, half of the optical emission from this region may well be blocked by very optically-thick material (e.g. the molecular torus). This is suggested by the fact that, in some other Seyfert nuclei, even infrared coronal lines are observed to be blueshifted with respect to the low-ionization narrow lines implying that any

redshifted coronal emission must be heavily extinguished. If this is the case, the true obscuration-corrected coronal line flux maybe twice that observed leading to a revised covering fraction of $f_c \approx 0.08$. This compares well with the estimate of the covering fraction of the outer warm absorber, $f_{owa} \sim 0.1$, based on the analysis of *ASCA* data for a sample of Seyfert galaxies (Reynolds 1997).

According to our CLOUDY calculations, the observed [FeXI]λ7892 emission cannot be explained as originating from the same material as the other coronal lines. Within our hypothesis, three possibilities present themselves. First, the observed [FeXI]λ7892 may have its origins elsewhere. Any separate coronal line emitting component would then be heavily constrained by the fact that it could not overproduce [FeX]λ6375 and [FeXIV]λ5303. Secondly, the uncertainties in the atomic physics may lead CLOUDY to grossly underestimate the [FeXI]λ7892 flux and this line may, in fact, originate within the same material as the other coronal lines. Thirdly, the uncertainties in the atomic physics may have led CLOUDY to grossly overestimate the [FeX]λ6375 and [FeXIV]λ5303 emission from the outer warm absorber. In this case, either the warm absorber covering fraction is large ($f_c \gtrsim 0.1$) or the coronal lines are emitted from a completely distinct (and as yet unidentified) region. Further progress in this area clearly requires better atomic parameters for these transitions, such as those which will be provided by the IRON project (Hummer et al. 1993).

6   FURTHER DISCUSSION

6.1   Polarization

Several authors have noted a high degree of polarization in the optical/IR spectrum of MCG−6-30-15 (e.g. Thompson & Martin 1988; Brindle et al. 1990). Polarization fractions of 4–6 per cent have been observed, with a slight tendency towards increasing polarization with decreasing wavelength. This is a significantly larger polarization than is typically found in Seyfert nuclei. The polarization is found to be aligned with the major axis of the host galaxy.

There are two possible causes for this polarization (see Kartje 1995 for a recent review of polarization mechanisms in AGN). First, a large scale alignment of dust grains along the line of sight to the central source can produce polarization via dichroic extinction (i.e. one polarization is preferentially scattered out of the line of sight by the dust grains). Secondly, scattering of flux into the observers line of sight by dust or free electrons will naturally produce polarization. In MCG−6-30-15 we have independent evidence for both scattering and the presence of line-of-sight dust. Thus, both of these mechanisms may be relevant – careful spectropolarimetry and detailed modeling will be needed to disentangle these effects.

We note that IRAS 13349+2438, the other good dusty-warm absorber candidate, also displays a very high degree of polarization (about 8 per cent). Wills et al. (1992) have found that the spectrum of the polarized light is typical of an unreddened AGN, thereby suggesting that the polarization is primarily due to scattering of the flux along a relatively dust-free path into the observers line-of-sight.

6.2 Global energetics

Using the estimated unreddened spectrum, we can address the issue of the energy distribution/flow in this source. Here, we shall assume a reddening of $E(B-V) = 0.61$, leading to the unreddened spectrum sketched in Fig. 4. The (isotropic) luminosity in the 0.1–1000 keV band is then

$$L(\text{X} - \text{ray}/\gamma-\text{ray}) \sim 2 \times 10^{43}\,\text{erg}\,\text{s}^{-1}\,, \qquad (17)$$

the NIR/optical/UV luminosity is

$$L(\text{NIR/optical/UV}) \sim 2 \times 10^{43}\,\text{erg}\,\text{s}^{-1}\,, \qquad (18)$$

and the MIR/FIR luminosity is

$$L(\text{MIR/FIR}) \sim 4 \times 10^{43}\,\text{erg}\,\text{s}^{-1}\,. \qquad (19)$$

The NIR/optical/UV luminosity given here is really a lower-limit since we have assumed the minimum possible value for the reddening. These waveband groups have been chosen on the basis of physical origin. The X-ray/γ-ray (i.e. $\sim 2 \times 10^{16}$ Hz and above) emission is thought to be produced by non-thermal processes (e.g. Comptonization) in a hot corona associated with the inner regions of an accretion disk. The NIR/optical/UV ($\sim 10^{14}-10^{16}$ Hz) emissions have plausible origins as thermal emission from the optically-thick accretion disk material. The MIR/FIR ($\sim 10^{12} - 10^{14}$ Hz) emission is likely to be thermal emission from warm or hot dust associated with the dusty warm absorber and putative molecular torus. Here we address the implications of the relative magnitudes of these luminosities for the energetics of the source.

First, we will discuss some theoretical expectations. We will assume a pure black hole model for the AGN emission, i.e. we will assume no contribution to the observed 'AGN' emission from a nuclear star-cluster or starburst. As mentioned in the Introduction, it is believed that the inner accretion disk possesses a hot optically-thin corona responsible for the non-thermal X-ray/γ-ray emission. Coronal models coupled with spectral constraints imply that a large fraction of the energy that is (locally) dissipated in the accretion disk is transported into the corona, possibly in a magnetic form, before being radiated. The dominant radiation process is thought to be inverse Compton scattering of soft thermal (optical/UV) photons from the accretion disk. The emission of the optical/UV seed photons is probably driven by high-energy irradiation from the corona, thereby completing a self-sustaining feedback.

Suppose that the corona covers the entire disk surface and that almost all of the accretion energy is released within the corona leading to the X-ray/γ-ray power-law emission. Approximately half of the primary high-energy photons will strike the accretion disk. Approximately half of the coronal[‡] flux that strikes the disk will be thermalized and re-radiated at optical/UV wavelengths, with the remaining half being 'reflected' (i.e. the photons undergo Compton backscattering or excite X-ray fluorescence). Thus, this scenario would predict

$$L(\text{NIR/optical/UV}) = \Lambda L(\text{X} - \text{ray}/\gamma-\text{ray}). \qquad (20)$$

where $\Lambda \sim 1/3$. Observationally, we infer there to be significantly more NIR/optical/UV emission than this, $\Lambda \gtrsim 1$ (where approximate equality corresponds to the case where the reddening takes its minimum allowed value, $E(B-V) = 0.61$). There are several possible interpretations. First, only a fraction of the (locally) dissipated energy may be transported into the corona. However, it is difficult to reconcile this with the X-ray spectrum given current coronal models (e.g., Haardt & Maraschi 1991). Secondly, there may be another optical/UV source in addition to the accretion disk such as a powerful nuclear starburst. This is difficult to reconcile with the fact that the optical continuum shown in Fig. 2a appears featureless and reddened to the same degree as the BLR. Lastly, and most likely, the corona may not cover the whole disk. It may be patchy or only exist in the innermost regions of the disk. The regions of the accretion disk without an active corona would still produce optical/UV emission via thermal emission resulting from viscous dissipation.

For the minimal reddening case, $E(B - V) = 0.61$, the MIR/FIR luminosity is comparable with luminosity in the whole of the rest of the spectrum. Within the dust-reprocessing paradigm, this is a troublesome result to understand unless the covering fraction of the dusty material is almost unity or the primary emission is anisotropic (with more primary radiation being emitted towards the dusty reprocessing material than towards us). A covering fraction of unity is implausible given our understanding of the geometry of a Seyfert nucleus. However, if we suppose that $E(B - V) > 0.61$, then the IR/optical/UV luminosity can greatly exceed the above value thereby alleviating the problem of the MIR/FIR production.

7 CONCLUSIONS

We have presented a multiwaveband study of the Seyfert 1 galaxy MCG−6-30-15, including previously unpublished optical data from the AAT, and UV data from *IUE*. Our compilation of data, spanning 6 decades of frequency, has allowed us to examine reprocessing mechanisms and the geometry of this system.

The optical line and continuum emission both show the effects of dust extinction. The reddening inferred from Balmer line studies lies in the range $E(B-V) = 0.61-1.09$. Given this reddening, we would expect the UV emission from the source to be less than observed. The fact that we do detect a UV continuum and broad C IVλ1549 line can be reconciled with a typical Seyfert spectrum if 1–5 per cent of the intrinsic (i.e. dereddened) source spectrum is scattered around the matter responsible for the extinction and into our line of sight. UV spectropolarimetry will be required to test this hypothesis.

The X-ray spectrum of this Seyfert nucleus clearly reveals a warm absorber but little of the cold (neutral) absorption that would be expected to accompany the dust responsible for the optical/UV reddening. To reconcile the X-ray absorption with the optical reddening we postulate that the dust resides in the warm absorber. Detailed X-ray studies have shown the warm absorber to be comprised of at least

---

[‡] In this context, the term 'coronal flux' is used to mean that radiation which is associated with the X-ray emitting disk-corona, and is unrelated to the 'coronal line emission' discussed in Section 5.

two-zones – an inner warm absorber at distances characteristic of the BLR and an outer warm absorber at distances characteristic of the putative molecular torus. Dust cannot survive in the inner warm absorber due to the intense radiation field – thus, the dust must reside in the outer absorber. We have examined photoionization models of the dusty (outer) warm absorber. Upon comparing such models with *ASCA* spectra we find evidence for non-standard dust mixtures, although the current data to not allow us to pursue this issue in detail.

The optical spectrum of MCG−6-30-15 displays the high-excitation forbidden lines of [FeX]λ6375, [FeXI]λ7892 and [FeXIV]λ5303, the so-called coronal lines. As is often found in other Seyfert nuclei, these lines have widths that are intermediate between those of the broad Balmer lines and the lower-excitation forbidden lines. Photoionization modeling with CLOUDY suggests that the CLR may be identified with the outer warm absorber.

REFERENCES

Alloin D. et al.,1995, A&A, 293, 293
Barvainis R., 1987, ApJ, 320, 537
Berriman G., 1989, ApJ, 345, 713
Brandt W. N., Fabian A. C., Pounds K. A., 1996, MNRAS, 278, 326
Brindle C., Hough J. H., Bailey J. A., Axon D. J., Ward M. J., Sparks W. B., McLean I. S., 1990, MNRAS, 280, 823
Burke J. R., Silk J., 1974, MNRAS, 190, 1
Canfield R. C., Puetter R. C., 1981, ApJ, 243, 381
Cappi M., Matsuoka M., Comastri A., Brinkmann W., Elvis M., Palumbo G. G. C., Vignali C., 1997, AJ, in press
Collin-Souffrin S., Dyson J. E., McDowell J. C., Perry J. J., 1988, MNRAS, 232, 539
Crenshaw D. M. et al., 1996, ApJ, 470, 322
Edelson R. A. et al., 1996, ApJ, 470, 364
Espey B. R., Carswell R. F., Bailey J. A., Smith M. G., Ward M. J., 1989, ApJ, 342, 666
Fabian A. C. et al. 1994a, PASJ, 46, L59
Fabian A. C. et al. 1995, MNRAS, 277, L11
Ferland G.L., 1991, Ohio State University, Astronomy Department Internal Report 91-01
Field G. B., Rogers R. D., 1993, ApJ, 403, 94
George I. M., Fabian A. C., 1991, MNRAS, 249, 352
Grandi S. A., 1978, ApJ, 221, 501
Guiricin G., Mardirossian F., Mezzetti M., 1995, 446, 550
Guilbert P. W., Rees M. J., 1988, MNRAS, 233, 475
Haardt F., Maraschi L., 1991, ApJ, 380, L51
Halpern J.P., 1984, ApJ, 281, 90
Heiles C., Kulkarni S., Stark A. A., 1981, ApJ, 247, 73
Hummer D. G., Berrington K. A., Eissner W., Pradhan A. K., Saraph H. E., Tully J. A., 1993, A&A, 279, 298
Iwasawa K. et al., 1996, MNRAS, 282, 1038
Kartje J. F., 1995, ApJ, 452, 565
Kaspi S. et al., 1996, ApJ, 470, 322
Korista K. T. et al., 1995, ApJS, 97, 285
Kwan J. Y., Krolik J. H., 1981, ApJ, 250, 478
Lightman A. P., White T. R., 1988, ApJ, 335, 57
Malkan M. A., 1983, ApJ, 264, L1
Mathur S., Elvis M., Wilkes B., 1995, ApJ, 452, 230
Matt G., Perola G. C., Piro L., 1991, A&A, 245, 63
Morris S. L., Ward M. J., 1988, MNRAS, 230, 639
Nandra K., Pounds K.A., 1992, Nat, 359, 215
Nandra K., Pounds K. A., Stewart G. C., 1990, MNRAS, 242, 660
Oliva E., 1996, to appear in IAU Colloquium 159, Emission lines in Active Galaxies:New Methods and Techniques.
Oliva E., Salvati M., Moorwood A. F. M., Marconi A., 1994, A&A, 288, 457
Osterbrock D. E., 1989, Astrophysics of Gaseous Nebulae and Active Galactic Nuclei, University Science Books, Mill Valley
Osterbrock D. E., Fulbright J. P., 1996, PASP, 108, 183
Otani C. et al., 1996, PASJ, 48, 211
Pineda F. J., Delvaille J. P., Huchra J., Davis M., 1978, IAU Circ., 3202.
Pineda F. J., Delvaille J. P., Grindlay J. E., Schnopper H. W., 1980, 237, 414
Pounds K. A., Nandra K., Stewart G. C., George I. M., Fabian A. C., 1990, Nat, 344, 132
Rees M. J., 1984, ARAA, 22, 471
Reichert G. A. et al., 1994, ApJ, 425, 582
Reynolds C. S., 1996, PhD thesis, Univ. of Cambridge.
Reynolds C. S., 1997, MNRAS, in press
Reynolds C. S., Fabian A. C., 1995, MNRAS, 273, 1167
Reynolds C. S., Fabian A. C., Nandra K., Inoue H., Kunieda H., Iwasawa K., 1995, MNRAS, 277, 901
Shull M. J., Van Steenberg M., 1982, ApJS, 48, 95
Stirpe G. M. et al., 1994, ApJ, 425, 609
Tanaka Y. et al., 1995, Nat, 375, 659
Thompson I. A., Martin P. G., 1988, ApJ, 330, 121
Ward M. J., Elvis M., Fabbiano G., Carleton N. P., Willner S. P., Lawrence A., 1987, ApJ, 315, 74
Wills B. J., Wills D., Evans N. J., Natta A., Thompson K. L., Breger M., Sitko M. L., 1992, ApJ, 400, 96
Wu C.-C., Boggess A., Gull T. R., 1983, ApJ, 266, 28
Zdziarski A. A., Fabian A. C., Nandra K., Celotti A., Rees M. J., Done C., Coppi P. S., Madejski G. M., 1994, MNRAS, 269, 55